Synthesis of arbitrarily discrete, diffractionless beams using dual-wavelength diffractive objective lens for optical pickup head

Hui-Hsiung Lin[1,2,*] and Mao-Hong Lu[1]

[1]*Department of Photonics and Institute of Electro-Optical Engineering, National Chiao Tung University, Hsinchu, Taiwan 300, Republic of China*

[2]*Mechanical and Systems Research Laboratories, Industrial Technology Research Institute, Chutung, Hsinchu, Taiwan 310, Republic of China*

** phranklin@hotmail.com*

Abstract: Sensitivity to disk vibration and large component number, which complicates assembly and optical alignment, are the drawbacks of traditional optical pickup systems. Here, a numerical method of designing a dual-wavelength diffractive objective lens with high numerical aperture for generating arbitrarily discrete, diffractionless beams with extended depth of focus is presented. Simulation and experimental results show that the optimized design provides better resolution, longer depth of focus and higher diffractive efficiency. The proposed design is promising for next-generation optical pickup systems that are more robust to disk vibration and easier to assemble.

©2010 Optical Society of America

OCIS codes: (050.1970) Diffractive optics; (100.5070) Phase retrieval; (230.3990) Micro-optical devices.

References and Links

1. R. M. Herman, and T. A. Wiggins, "Production and uses of diffractionless beams," J. Opt. Soc. Am. A **8**(6), 932–942 (1991).
2. L. C. Laycock, and S. C. Webster, "Bessel beams: their generation and application," GEC J. Res. **10**, 36–51 (1992).
3. J. H. McLeod, "Axicons and their uses," J. Opt. Soc. Am. A **50**(2), 166 (1960).
4. T. Hidaka, "Generation of a diffraction-free laser beam using a specific Fresnel zone plate," Jpn. J. Appl. Phys. **30**(Part 1, No. 8), 1738–1739 (1991).
5. M. Rioux, R. Tremblay, and P. A. Bélanger, "Linear, annular, and radial focusing with axicons and applications to laser machining," Appl. Opt. **17**(10), 1532–1536 (1978).
6. Z. Ding, H. Ren, Y. Zhao, J. S. Nelson, and Z. Chen, "High-resolution optical coherence tomography over a large depth range with an axicon lens," Opt. Lett. **27**(4), 243–245 (2002).
7. V. E. Peet, and R. V. Tsubin, "Third-harmonic generation and multiphoton ionization in Bessel beams," Phys. Rev. A **56**(2), 1613–1620 (1997).
8. J. Sochacki, S. Bará, Z. Jaroszewicz, and A. Kołodziejczyk, "Phase retardation of the uniform-intensity axilens," Opt. Lett. **17**(1), 7–9 (1992).
9. Z. Jaroszewicz, and J. Morales, "Lens axicons: systems composed of a diverging aberrated lens and a perfect converging lens," J. Opt. Soc. Am. A **15**(9), 2383–2390 (1998).
10. J. Durnin, "Exact solutions for nondiffracting beams. I. The scalar theory," J. Opt. Soc. Am. A **4**(4), 651–654 (1987).
11. L. Niggl, T. Lanzl, and M. Maier, "Properties of Bessel beams generated by periodic gratings of circular symmetry," J. Opt. Soc. Am. A **14**(1), 27–33 (1997).
12. A. J. Cox, and D. C. Dibble, "Nondiffracting beam from a spatially filtered Fabry-Perot resonator," J. Opt. Soc. Am. A **9**(2), 282–286 (1992).
13. N. Davidson, A. A. Friesem, and E. Hasman, "Holographic axilens: high resolution and long focal depth," Opt. Lett. **16**(7), 523–525 (1991).
14. B. Z. Dong, G. Z. Yang, B. Y. Gu, and O. K. Ersoy, "Iterative optimization approach for designing an axicon with long focal depth and high transverse resolution," J. Opt. Soc. Am. A **13**(1), 97–103 (1996).
15. J. Rosen, B. Salik, and A. Yariv, "Pseudo-nondiffracting beams generated by radial harmonic functions," J. Opt. Soc. Am. A **12**(11), 2446–2457 (1995).

#119710 - $15.00 USD Received 10 Nov 2009; revised 27 Dec 2009; accepted 7 Jan 2010; published 22 Jan 2010

16. J. Rosen, B. Salik, A. Yariv, and H. K. Liu, "Pseudonondiffracting slitlike beam and its analogy to the pseudonondispersing pulse," Opt. Lett. **20**(5), 423–425 (1995).
17. R. Liu, B. Y. Gu, B. Z. Dong, and G. Z. Yang, "Diffractive phase elements that synthesize color pseudo-nondiffracting beams," Opt. Lett. **23**(8), 633–635 (1998).
18. B. E. A. Saleh, and M. C. Teich, *Fundamentals of Photonics* (Wiley, New York, 1991), pp. 131.
19. H. H. Lin, and M. H. Lu, "Dual-Wavelength Membrane-Based Diffractive Optical Element with Extended Depth-of-Focus for Optical Pickup Head," Jpn. J. Appl. Phys. **46**(No. 8B), 5485–5493 (2007).
20. J. W. Goodman, *Introduction to Fourier Optics* (McGraw-Hill, New York, 1996), 2nd ed., pp. 66.
21. R. Fletcher, *Practical Methods of Optimization* (Wiley, New York, 1999), 2nd ed., pp. 6–92.
22. M. W. Farn, and J. W. Goodman, "Effect of VLSI fabrication errors on kinoform efficiency," Proc. SPIE **1211**, 125–136 (1990).
23. J. A. Cox, T. R. Werner, J. C. Lee, S. A. Nelson, B. S. Fritz, and J. W. Bergstrom, "Diffraction efficiency of binary optical elements," Proc. SPIE **1211**, 116–124 (1990).
24. M. Holz, M. B. Stern, S. Medeiros, and R. E. Knowlden, "Testing binary optics: accurate high-precision efficiency measurements of microlens arrays in the visible," Proc. SPIE **1514**, 75–89 (1991).

1. Introduction

An optical pickup head generally comprises one or more laser sources and an objective lens that must focus the laser beam onto a disk of specific overcoat thickness. The lens must create a single aberration-free spot on different types of disk media, which spin at high speed and tend to wobble and vibrate. The focal length of the objective lens may also vary slightly during operation, and these variations may be either discrete or continuous. Therefore, a large depth of focus and a small spot size are critical. Furthermore, a large depth of focus in the neighborhood of the disk media is necessary when using one lens to focus multiple laser sources of different wavelengths, as a change in wavelength implies a change in focal length.

Consequently, objective lenses must have a large depth of focus and high lateral resolution. But as is well known, conventional elements (spherical lenses, mirrors, etc.) cannot have both the features simultaneously: a large lateral resolution requires a large numerical aperture (NA), whereas a large depth of focus requires a small NA. A nondiffracting beam such as a zero-order Bessel beam can form a narrow focal line along the optical axis with a very large (compared with Rayleigh range) depth of focus. Such beams have a number of applications such as in precision alignment [1,2], profile measurement, industrial inspection, information display [3], laser surgery [4], laser machining [5], optical coherence tomography [6], and harmonic generation [7]. In fact, many different types of optical elements can be used to generate nondiffracting beams: conic mirrors [8], axicons [9,10], circular gratings [11], Fabry-Perot etalons [12], holograms [13], and diffractive axicons [14].

A more recent development is the concept of pseudo-nondiffracting beams [15–17], characterized by an almost constant axial intensity distribution over a finite axial region, beamlike shape in the transverse direction, and operation in the far field. But almost all research [11–17] conducted thus far on nondiffracting beams—whether of single or multiple segments, or with monochromatic or multiple-wave illumination—have been devoted to optical systems with NA [18] ($=1.22\lambda/S$, where S is the diameter spot-size for the Airy criterion) of approximately 0.005–0.07. To our knowledge, no reports exist on the generation of nondiffracting beams in a dual-wavelength optical pickup head system with a diffractive objective lens (DOL) of high NA and arbitrarily extended depth of focus. This paper describes the design of such a high-NA DOL that can generate arbitrarily discrete, diffractionless beams (ADDB) at multiple wavelengths for an optical pickup head, which is an advanced design for previous study [19]. Because of the large NA, the focal length is very near the front-zone of the near-field diffraction region. Further, incorporating this DOL, an optimized optical pickup head design for digital versatile disks (DVDs) is proposed. The ADDBs of two wavelengths have a high transverse resolution and a segmented axial intensity distribution with a single wavelength in each section, besides an extended depth of focus. The design of a high NA

#119710 - $15.00 USD Received 10 Nov 2009; revised 27 Dec 2009; accepted 7 Jan 2010; published 22 Jan 2010
(C) 2010 OSA

DOL with dual-wavelength ADDBs for an optical pickup head was conducted using a conjugate-gradient method.

Our analysis shows that the optimized design should increase beam convergence and decrease nonuniformity in the axial intensity by several orders compared with previous designs [14,17]. Further, such a lens was fabricated and integrated into an optical measurement system with dual-wavelength Laser source. Both our calculation and measurement confirms the increased lateral resolution and expanded longitudinal axial distribution, which has a potential to overcome the problems in assembly and optical alignment of conventional designs.

2. Design and optimization

To generate the dual-wavelength ADDB functions for a DVD optical pickup head, we propose a modified numerical optimization method to design a fused-silica based DOL objective lens with high NA. Dual-wavelength ADDBs are characterized by segmented axial intensity distributions and high transverse resolutions, with each segment having an ultra-long depth of focus, high NA and single wavelength. The proposed numerical optimization is derived from the conjugate-gradient method, which integrates a high-order Bessel modified function. Because of the very short focal length, the DOL approaches the near-field diffraction limit. Consequently, the integral function of the Bessel term, which is classified in the linear transfer equation of the Fresnel diffraction integral function in the paraxial approximation, cannot be neglected. But this method leads to a slow convergence and a large computing load during simulation, which can be solved by using a high-order Bessel modified error function with a 2-D weighting factor.

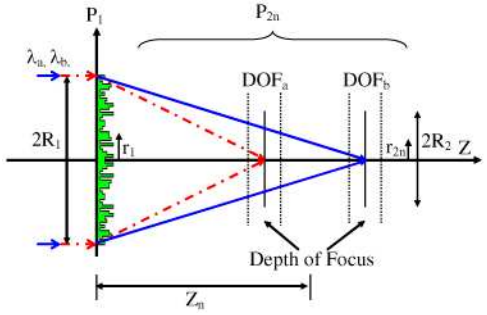

Fig. 1. Schematic diagram of dual-wavelength ADDB diffractive optical system that approaches the front-zone of the near-field diffraction region.

The DOL is placed on the input plane of the system. The incident light passes through the DOL and propagates in free space, as illustrated in Fig. 1, where r_1 and r_{2n} denote the radial coordinates on the input and nth sampling planes, respectively. R_1 and R_2 denote the radius on the input and output planes, respectively. The input field distribution on the incident plane (Z = 0) is given by

$$U_1(\lambda_m, r_1) = \rho_1(\lambda_m, r_1)\exp\left[i\phi_1(\lambda_m, r_1)\right], \tag{1}$$

where $\phi_1(\lambda_m, r_1)$ is the phase function of the incident plane wave, and $\rho_1(\lambda_m, r_1)$ is the amplitude distribution of the incident light for wavelength component λ_m. $h(r_1)$ represents the distribution of the surface-relief depth of the DOL, which is expressed as

$$\phi_1(\lambda_m, r_1) = \frac{2\pi}{\lambda_m}\left[n(\lambda_m) - 1\right]h(r_1). \tag{2}$$

#119710 - $15.00 USD Received 10 Nov 2009; revised 27 Dec 2009; accepted 7 Jan 2010; published 22 Jan 2010
(C) 2010 OSA

The corresponding output wave distribution function on the *n*th axial sampling plane located at Z_n is expressed by

$$U_2\left(\lambda_m, r_{2n}, Z_n\right) = \rho_2\left(\lambda_m, r_{2n}, Z_n\right)\exp\left[i\phi_2\left(\lambda_m, r_{2n}, Z_n\right)\right], \tag{3}$$

where $\phi_2\left(\lambda_m, r_{2n}, Z_n\right)$ is the phase function of the output wave, and $\rho_2\left(\lambda_m, r_{2n}, Z_n\right)$ is the amplitude distribution of the output light for wavelength component λ_m. In the Fresnel approximation [20], the high-order Bessel modified output field distribution along the optical axis at distance Z_n from the DOL can be expressed as

$$U_2\left(\lambda_m, r_{2n}, Z_n\right) = \frac{2\pi}{i\lambda_m Z_n}\exp\left(\frac{i2\pi Z_n}{\lambda_m}\right)\times\int_0^{R_1}\rho_1\left(r_1, \lambda_m\right)\exp\left\{i\frac{2\pi}{\lambda_m}\left[n\left(\lambda_m\right)-1\right]h\left(r_1\right)\right\}$$

$$\times\exp\left[\frac{i\pi\left(r_1^2+r_{2n}^2\right)}{\lambda_m Z_n}\right]\times J_0\left(\frac{2\pi r_1 r_{2n}}{\lambda_m Z_n}\right)r_1 dr_1, \tag{4}$$

where R_1 is the maximum radius of the DOL, and J_0 is the zero-order Bessel function of the first kind. The focal length of the DOL for the optical pickup head is very short (within 1.8–2.4 mm), considerably less than that reported in the previous descriptions of conventional Bessel beams. Consequently, the integral function of the Bessel term cannot be omitted in free space. The axial intensity distribution can be presented by selecting a trapezoid profile. The performance of the designed DOL is evaluated by using a high-order Bessel modified error function E with a two-dimensional weighting factor $W(\lambda_m, r_{2p}, Z_n)$:

$$E = \sum_{m=1}^{N_\lambda}\sum_{p=1}^{N_{2n}}\sum_{n=1}^{N_z} W\left(\lambda_m, r_{2p}, Z_n\right)\left[\tilde{\rho}_2\left(\lambda_m, r_{2p}, Z_n\right)-\left|U_2\left(\lambda_m, r_{2p}, Z_n\right)\right|\right]^2, \tag{5}$$

$$W\left(\lambda_m, r_{2p}, Z_n\right) = \begin{cases} \dfrac{1-W_{\min}}{N_S\left(r_{2p}, Z_n\right)} & signal \quad zone \\ \dfrac{W_{\min}}{N_z\left(r_{2p}, Z_n\right)-N_S\left(r_{2p}, Z_n\right)}, & non-signal \quad zone \end{cases}, \tag{6}$$

where $N_s\left(r_{2p}, Z_n\right)$ is the number of sampling points in the signal zone of the output Z axis and output plane, and $N_Z\left(r_{2p}, Z_n\right)$ is the total number of sampling points on the output Z axis and the output plane. W_{min} is the minimum weighting value.

In the conjugate-gradient method [21], the solution to the unknown variable $y(r_1)$, search direction $d^{(k)}$, and factor $\beta^{(k-1)}$ can be derived from an iteration algorithm of the form

$$y^{(k+1)}\left(r_1\right) = y^{(k)}\left(r_1\right) + \tau^{(k)}\vec{d}^{(k)}, \tag{7}$$

where $\tau^{(k)}$ and vector $d^{(k)}$ are the step size and search direction in the *k*th iteration, respectively. The search direction $d^{(k)}$ is given by

$$\vec{d}^{(k)} = -\vec{\nabla}E\left[y^{(k)}\left(r_1\right)\right] + \beta^{(k-1)}\vec{d}^{(k-1)}, \tag{8}$$

and the factor $\beta^{(k-1)}$ can be expressed as

#119710 - $15.00 USD Received 10 Nov 2009; revised 27 Dec 2009; accepted 7 Jan 2010; published 22 Jan 2010
(C) 2010 OSA

$$\beta^{(k-1)} = \frac{\left|\vec{\nabla} E\left[y^{(k)}(r_1) \right]\right|^2}{\left|\vec{\nabla} E\left[y^{(k-1)}(r_1) \right]\right|^2}, \tag{9}$$

where $\nabla E[y^{(k)}(r_1)]$ is the gradient of error function E with respect to $y(r_1)$, and r_{2p} denotes the radial coordinates on the pth sampling plane. The step size $\tau^{(k)}$ is chosen such that $E[y^{(k+1)}(r_1)] < E[y^{(k)}(r_1)]$. To estimate the uniformity of the constant axial intensity distribution I over the given segment, we define nonuniformity in the expression as follow:

$$\text{Nonuniformity} = \frac{\sqrt{\langle I^2 \rangle - \langle I \rangle^2}}{\langle I \rangle}, \tag{10}$$

where $< >$ stands for the average value of the related intensity distribution over the given axial segment. The efficiency of the DOL is based on the ratio of two simulated or measured quantities, such as

$$\text{Efficiency} \equiv \text{Useful energy / Incident energy.} \tag{11}$$

As discussed by Goodman [22], we describe the DOL efficiency as a normalized Strehl efficiency, defined as the on-axis irradiance ratio η of the tested DOL to the irradiance ratio of a diffraction-limited ideal DOL,

$$\eta_s \equiv \eta_{\text{Tested DOL}} / \eta_{\text{Ideal DOL}}. \tag{12}$$

To normalize the Strehl ratio, we divide it by the ideal efficiency of the phase-quantized DOL. This ideal DOL efficiency has been derived by Dammann [22,23], as

$$\eta_{\text{Ideal DOL}} = \left[\frac{\sin\left(\frac{\pi}{2^n}\right)}{\frac{\pi}{2^n}} \right]^2, \tag{13}$$

where n is the number of masks, and 2^n the number of phase levels.

Experimentally, we can determine the efficiency $\eta_{\text{Tested DOL}}$ by normalizing the power in the simulation or measurement results [24],

$$\eta_{\text{Tested DOL}} \equiv E_u / E_i, \tag{14}$$

given by the ratio of the energy in the central lobes of the far-field pattern, E_u, to the incident energy E_i.

3. Numerical simulation

The phase of the dual-wavelength DOL was calculated by using the high-order Bessel modified conjugate-gradient method. According to the specifications of the DVD optical pickup head white paper (Table 1) and the requirement of our fabrication process, we determined the size and specifications of the DOL to satisfy the diffraction-limited criterion and tolerance of fabrication. Table 2 presents the specifications of the dual-wavelength ADDB DOL for DVD optical pickup head. We carried out the design of a DOL that generated dual-wavelength ADDB with two segments, each segment being monochromatic with wavelengths λ_{DVD} = 650 nm for the first segment and λ_{CD} = 780 nm for the second segment, respectively. From experience, we assigned high weights to the signal region with a constant axial intensity and low weights to the other regions. Moreover, we found that the number of sampling points for the input plane (N_1) and output plane (N_2) possessed significant roles in the tricky process of convergence during the simulation. There were some restrictions on the

#119710 - $15.00 USD Received 10 Nov 2009; revised 27 Dec 2009; accepted 7 Jan 2010; published 22 Jan 2010
(C) 2010 OSA

two parameters N_1 and N_2. For example, the minimum feature size achievable in the fabrication determined the maximum value of N_1. On the other hand, if the values of N_1 and N_2 were too large, the computation became more complex because of the slower convergence and the high computing load.

Table 1. Specifications of the DVD optical pickup head white paper.

Specifications	DVD-ROM	CD-ROM
Laser wavelength (nm)	650	780
Track distance (μm)	0.74	1.6
Pit depth (μm)	0.12	0.11
Pit length (μm)	0.4	0.834
Pit width (μm)	0.32	0.6
Numerical aperture (N.A.)	0.6	0.45
Diameter spot-size (μm)	1.32	2.11

To improve the convergence of the optimized simulation and reduce the computing load, we decreased the restrictions on the initial conditions. In the initial simulation, we began with a small number of sampling points with N_2 being 30 along the output optical plane.. Following this, in the subsequent calculation process, we used more sampling points and replaced them with the results that had been calculated previously in the initial phase. Finally, the number of sampling points N_2 was increased to 1000 in the last simulation.

Table 2. Specifications of the dual-wavelength ADDB DOL for the objective lens of DVD optical pickup head.

Design parameters	Diameter		Depth-of-focus		Diameter spot-size	
	Input	Output	650 nm	780 nm	650 nm	780 nm
Design scale	4.20 mm	60 μm	±120 μm		1.20 μm	1.80 μm
			1.68–1.92 mm	2.28–2.52 mm		
Sampling rings/ points	600	1000	4	4	20	30

#119710 - $15.00 USD Received 10 Nov 2009; revised 27 Dec 2009; accepted 7 Jan 2010; published 22 Jan 2010
(C) 2010 OSA

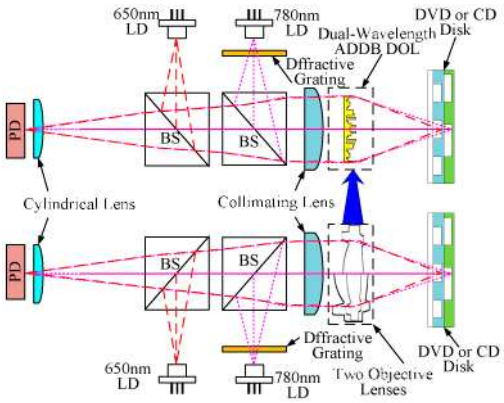

Fig. 2. Schematic illustration of objective lens for DVD optical pickup head system with dual-wavelength ADDB DOL.

A schematic illustration of the DOL that can generate a dual-wavelength ADDB for a DVD optical pickup head system is shown in Fig. 2. To present the utilization of this approach, we performed the design in two segments, where each segment retained its single wavelength feature: The first segment has a wavelength λ_{DVD} of 650 nm, a focal length of 1.8 mm, a depth-of-focus of ± 120 μm, and an the average spot-size diameter of 1.02 μm for the Airy criterion (NA ≈0.7775). The second segment had a wavelength λ_{CD} of 780 nm, a focal length of 2.4 mm, a depth-of-focus of ± 120 μm, and an average spot-size diameter of 1.59 μm for the Airy criterion (NA ≈0.5985). The plane wave consisting of these two wavelengths was incident upon the DOL. The sampling rings (points) N_1 was set to be 600 along the radial coordinate of the DOL within an aperture diameter of 4.2 mm. The spacing between adjacent axial sampling points N_z was chosen as 60 μm within an axial-intensity sampling distance of Z = 30 mm.

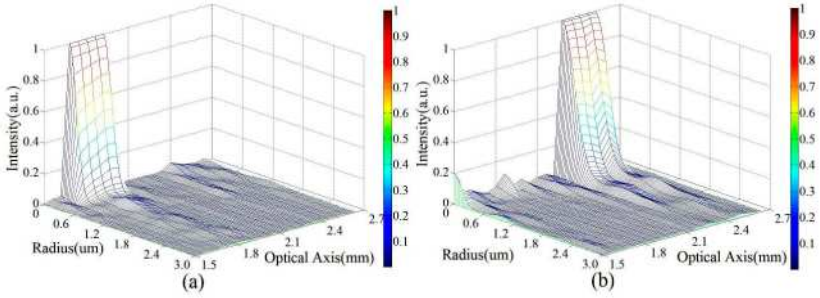

Fig. 3. Propagation of banded-krait-like beam and 3-D distribution of CP dual-wavelength ADDB DOL with two depth-of-focus regions: (a) λ = 650 nm DVD segment, (b) λ = 780 nm CD segment.

#119710 - $15.00 USD Received 10 Nov 2009; revised 27 Dec 2009; accepted 7 Jan 2010; published 22 Jan 2010
(C) 2010 OSA

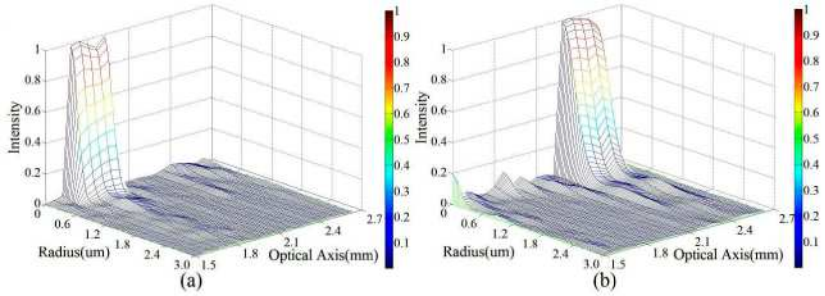

Fig. 4. Propagation of banded-krait-like beam and 3-D distribution of the sixteen-level quantization phase dual-wavelength ADDB DOL with two depth-of-focus regions: (a) λ = 650 nm, DVD segment; (b) λ = 780 nm, CD segment.

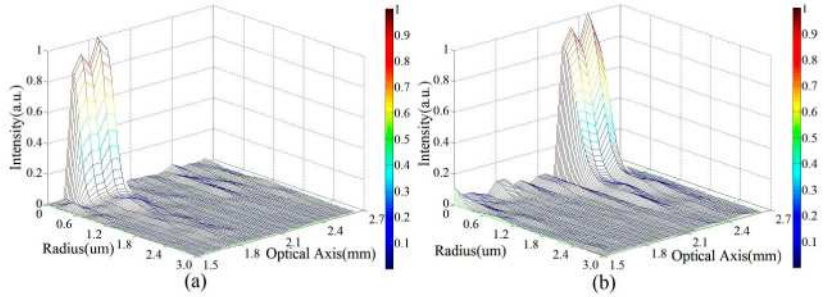

Fig. 5. Propagation of banded-krait-like beam and 3-D distribution of the eight-level quantization phase dual-wavelength ADDB DOL with two depth-of-focus regions: (a) λ = 650 nm, DVD segment; (b) λ = 780 nm, CD segment.

In the process of simulation, N_z was set to be 20 and chose the weighting factor W as 2. The total number of sampling points over the depth-of-focus region of constant axial intensity was 4–8 for λ_{DVD} = 650 nm and 14–18 for λ_{CD} = 780 nm. For λ_{DVD} = 650 nm, the nonuniformity was 4.899×10^{-4} within the depth-of-focus region [1.68 mm, 1.92 mm]. As sketched in Fig. 1, in which zone was represented by DOF_a; and for λ_{CD} = 780 nm, the nonuniformity was 6.325×10^{-4} within the depth-of-focus region [2.28 mm, 2.52 mm]. As schematized in Fig. 1, in which zone was indicated by DOF_b. To clearly illustrate the characteristics of the banded-krait-like beam shape of the dual-wavelength ADDB, the transverse intensity distributions for a continuous phase (CP) ADDB DOL in three-dimensional plots are shown in Figs. 3(a) and 3(b) for the λ_{DVD} segment and the λ_{CD} segment, respectively. Figures 4–5 illustrate the quantization-calculated 3-D propagation distribution results for a sixteen-level (16L) and an eight-level (8L) dual-wavelength ADDB DOL, respectively.

The average simulation results for the spot-size diameter required for the optimized dual-wavelength ADDB DOL are listed in Table 3. Despite the fact that the results for 8L were smaller than 16L or CP, the nonuniformity and efficiency for 8L was worse than that for 16L and CP. Figures 6–8 exhibit the spot-size diameter for the Airy criterion, $1/e^2$, and full width at half maximum (FWHM), which have continuous phases and quantized phases (16L and 8L), for designing the dual-wavelength ADDB DOL with two depth-of-focus regions (λ = 650 nm, DVD segment, and λ = 780 nm, CD segment). Notwithstanding the few side-lobe defects in certain output planes, the results of the simulations demonstrated a banded-krait-like beam shape with high transverse resolution for long-focal-depth characteristics. It is worth pointing out that the wavelength of each segment and depth-of-focus can be arbitrarily preset.

#119710 - $15.00 USD Received 10 Nov 2009; revised 27 Dec 2009; accepted 7 Jan 2010; published 22 Jan 2010
(C) 2010 OSA

Table 3. Simulated average spot-size diameter for the Airy criterion, $1/e^2$, and full width at half maximum (FWHM), which have continuous phases (CP) and quantization phases (16L and 8L), for designing the dual-wavelength ADDB DOL for the DVD optical pickup head.

λ (μm)	Goal of diameter spot size (Airy) μm	The average of simulation diameter spot size (Airy) μm			The average of simulation diameter spot size ($1/e^2$) μm			The average of simulation diameter spot size (FWHM) μm		
		CP	16L	8L	CP	16L	8L	CP	16L	8L
0.65	1.20	1.02	1.08	0.96	0.594	0.567	0.57	0.361	0.344	0.33
0.78	1.80	1.59	1.59	1.62	1.072	1.033	1.089	0.611	0.589	0.583

The surface-relief depth of the CP distribution for the designed ADDB DOL is illustrated in Fig. 9. The maximum surface-relief depth is H_T = 2.848 μm (for fused silica). These diagrams provided information of both the axial intensity uniformity and the transverse intensity distribution. It was conspicuously shown that the dual-wavelength ADDB characteristic exhibited a banded-krait-like beam shape with a high transverse resolution approaching the near-zone of the near-field diffraction region. The numerically simulated diffractive efficiencies for 16L and 8L fused-silica DOLs were 94.01% and 80.59% for λ_{DVD} = 650 nm, and 97.06% and 89.51% for λ_{CD} = 780 nm, respectively. Therefore, these simulation results verified that the DOL conformed to the requirements of long-focal-depths as well as high lateral resolution for application to DVD optical pickup heads.

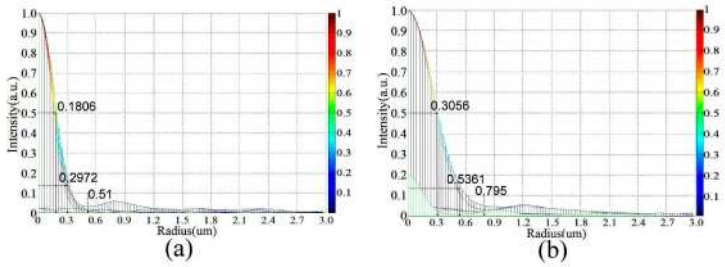

Fig. 6. Spot-size diameter of dual-wavelength ADDB DOL for the Airy criterion, $1/e^2$, and FWHM of CP for two depth-of-focus regions: (a) λ = 650 nm, DVD segment; (b) λ = 780 nm, CD segment.

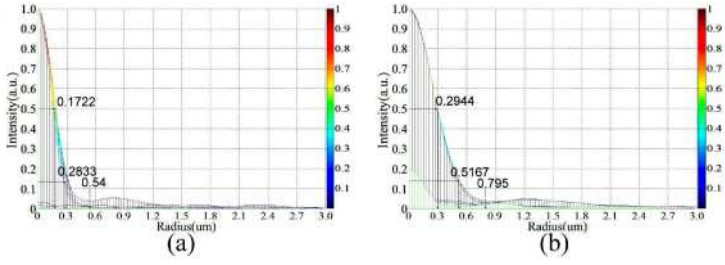

Fig. 7. Spot-size diameter of dual-wavelength ADDB DOL for the Airy criterion, $1/e^2$, and FWHM of the sixteen-level quantization phases of two depth-of-focus regions: (a) λ = 650 nm, DVD segment; (b) λ = 780 nm, CD segment.

#119710 - $15.00 USD Received 10 Nov 2009; revised 27 Dec 2009; accepted 7 Jan 2010; published 22 Jan 2010
(C) 2010 OSA

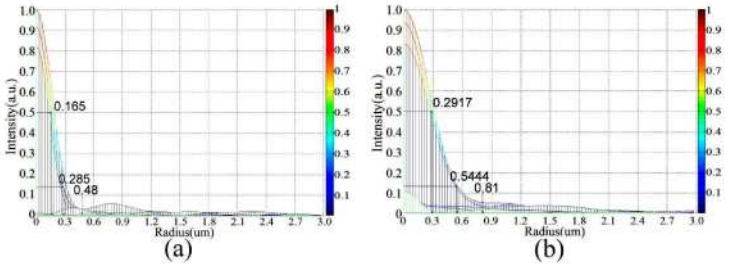

Fig. 8. Spot-size diameter of dual-wavelength ADDB DOL for the Airy criterion, $1/e^2$, and FWHM of the eight-level quantization phases of two depth-of-focus regions: (a) λ = 650 nm, DVD segment; (b) λ = 780 nm, CD segment.

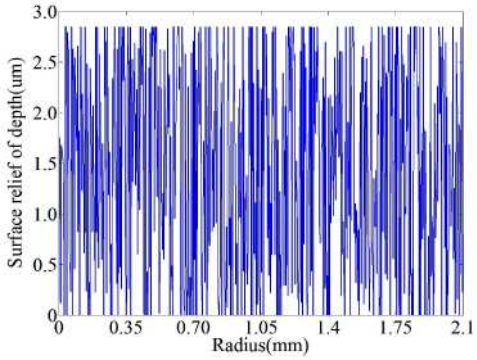

Fig. 9. Surface relief of depth of the CP distribution for the designed dual-wavelength ADDB DOL in DVD optical pickup heads.

4. Fabrication results

A fused-silica-based DOL with two wavelengths and a long depth of focus was fabricated by semiconductor micromachining techniques. The fabrication process involved reactive-ion etching to produce the surface relief structures on a flat quartz substrate. The three photo masks of the 8L for optical contact lithography contain 600 concentric circle rings, as shown in Fig. 10. Figure 11 shows a photograph of the fabricated fused-silica-based DOL. The minimum feature size is 3.5μm. Figure 12 shows a diagram of the surface relief structures viewed by scanning electron microscopy (SEM). Figures 13(a)–(d) show part of the surface relief structures on the finished DOL, measured by a Zygo 3D surface profiler measuring system. The diameter of the DOL was 4.2 mm. It is obviously seen from Fig. 12 that the DOL has some misalignment as a result of small residual defects in the fused-silica-based DOL. This may resulted in some differences between the theoretical calculation and actual measurements, unless the gray-scale lithography and alignment processes had been improved.

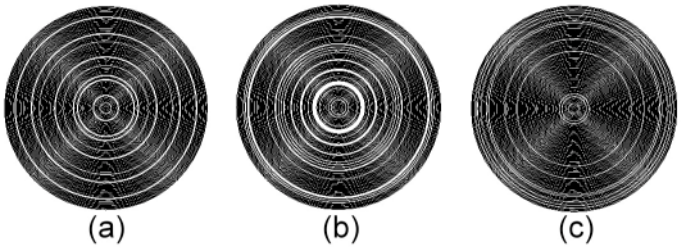

Fig. 10. Diagram illustrating the rings for (a) mask 1, (b) mask 2, and (c) mask 3 of the 8L for optical contact lithography contain 600 concentric circle rings.

#119710 - $15.00 USD Received 10 Nov 2009; revised 27 Dec 2009; accepted 7 Jan 2010; published 22 Jan 2010
(C) 2010 OSA

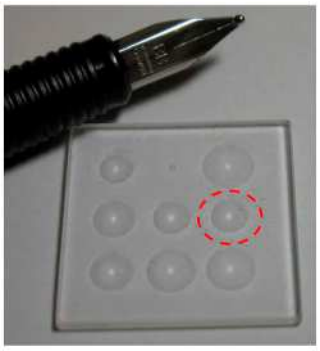

Fig. 11. The red dotted circle shows the fabricated fused-silica-based DOL with diameter of 4.2 mm and dual-wavelength ADDB.

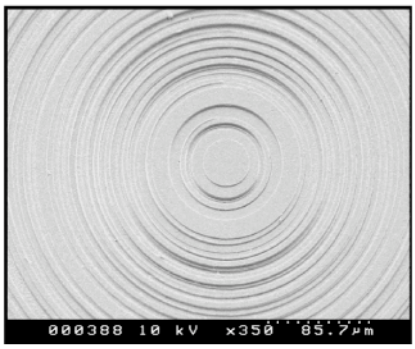

Fig. 12. SEM micrograph of surface relief structures on the fabricated fused-silica DOL with dual-wavelength ADDB.

5. Measurement results

The fabricated fused-silica DOL was tested on a dual-wavelength (652.5nm and 785.2nm) optical measurement system to verify the simulation results. Given the long depth-of-focus, a charge coupled device (CCD) camera was placed on an optical bench and moved along the optical axis to record the intensity (spot diagram) on the sampling planes, as shown in Fig. 14. The measured axial intensity distribution conspicuously indicated that there were slightly differences between the experimental and theoretical results. In Fig. 15, the FWHM spot size on planes at Z = 1.68, 1.72, 1.76, 1.80, 1.84, 1.88, and 1.92 mm, generated by the DOL are about 0.735, 0.833, 0.833, 0.882, 0.735, 0.784, and 0.784 μm, respectively. Figure 16 shows that the FWHM spot size in the CD segment on planes at Z = 2.28, 2.32, 2.36, 2.40, 2.44, 2.48, and 2.52 mm are about 1.078, 1.029, 1.029, 0.931, 1.127, 0.98, and 1.029 μm, respectively. These illustrations provided a view of both the axial intensity uniformity and the transverse intensity distribution. It was clearly seen that this dual-wavelength ADDB exhibited a banded-krait-like beam shape with a high transverse resolution, barring a few defects. These fabrication results indicated a view of both the transverse intensity distribution and the axial intensity uniformity, except for the spot size at Z = 2.44 mm.

#119710 - $15.00 USD Received 10 Nov 2009; revised 27 Dec 2009; accepted 7 Jan 2010; published 22 Jan 2010
(C) 2010 OSA

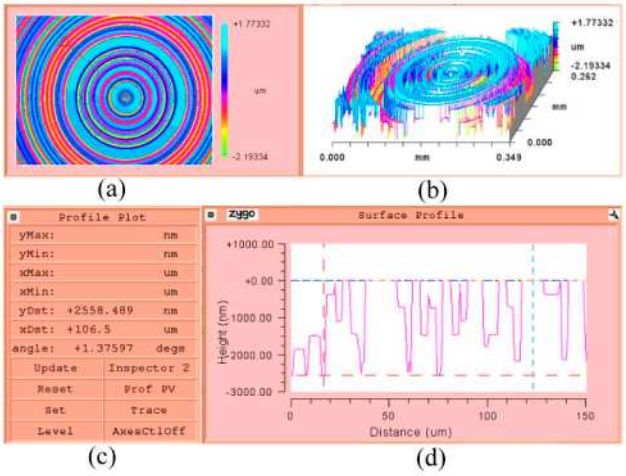

Fig. 13. Fabrication results for the dual-wavelength fused-silica-based ADDB DOL. The fractional profile in (a) 2-D, (b) 3-D, (c) measurement data, and (d) cross-section of the surface-relief structures of the 8L DOL (obtained on a Zygo 3-D surface profiler measuring system).

Although the fabricated fused-silica DOL had some alignment defects as a result of the mask misalignments and residual error, it is clear that the spot sizes and transverse resolutions were slightly insufficient for a DVD optical pickup system unless the fabrication processes had been improved. For example, better results can be achieved by using grey-levels or E-beam lithography to produce a smoother profile, which can achieve higher diffraction efficiency, smaller spot size, higher transverse resolution, and better axial intensity uniformity.

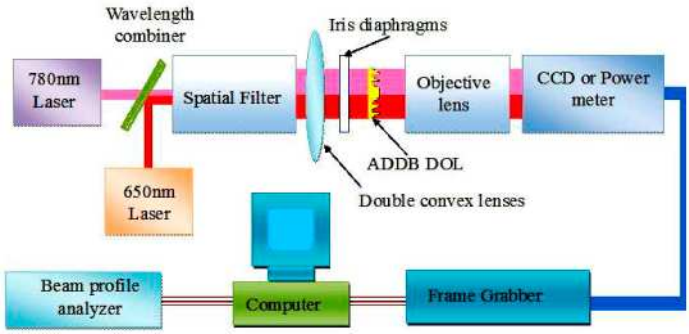

Fig. 14. Experimental setup for measuring the performance of the designed fused-silica-based DOL with dual-wavelength ADDB characteristic.

#119710 - $15.00 USD Received 10 Nov 2009; revised 27 Dec 2009; accepted 7 Jan 2010; published 22 Jan 2010
(C) 2010 OSA

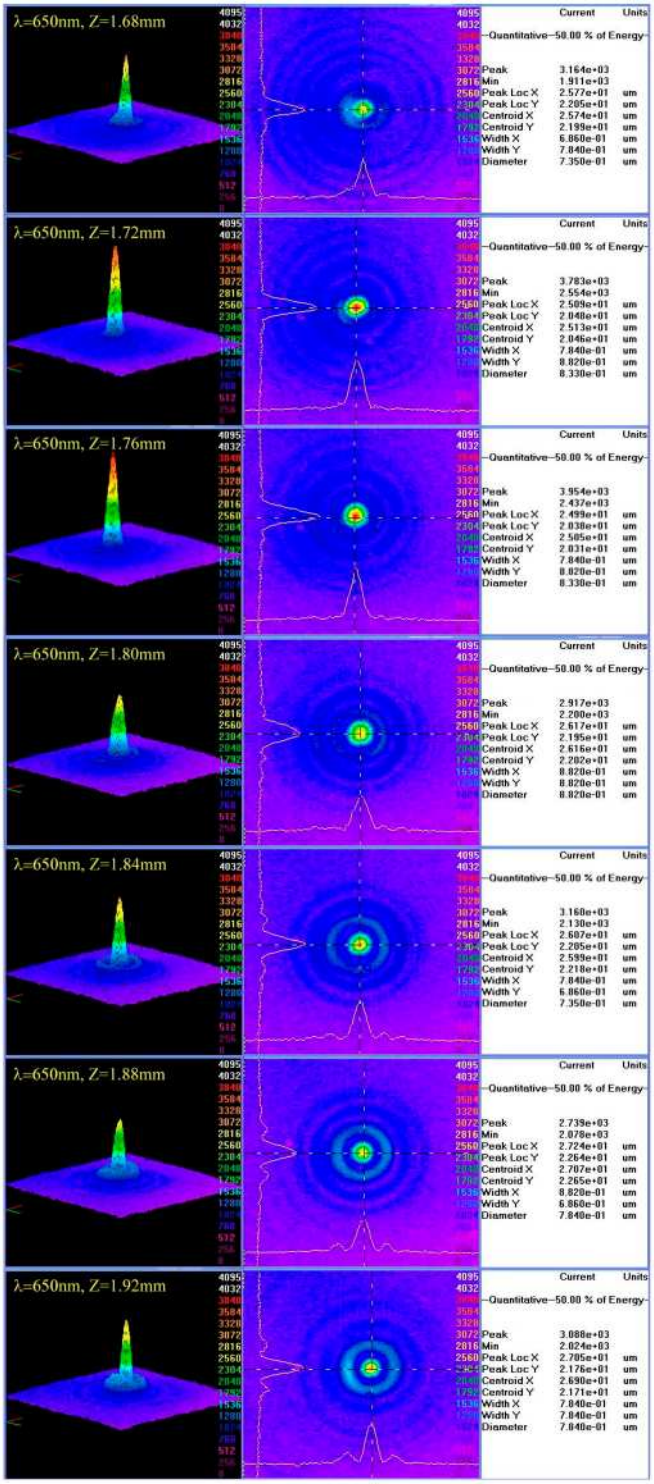

Fig. 15. Photographs present the spot size of the fused-silica-based DOL with dual-wavelength ADDB for FWHM of λ_{DVD} segment for a measuring distance of 40 μm per frame.

#119710 - $15.00 USD Received 10 Nov 2009; revised 27 Dec 2009; accepted 7 Jan 2010; published 22 Jan 2010
(C) 2010 OSA

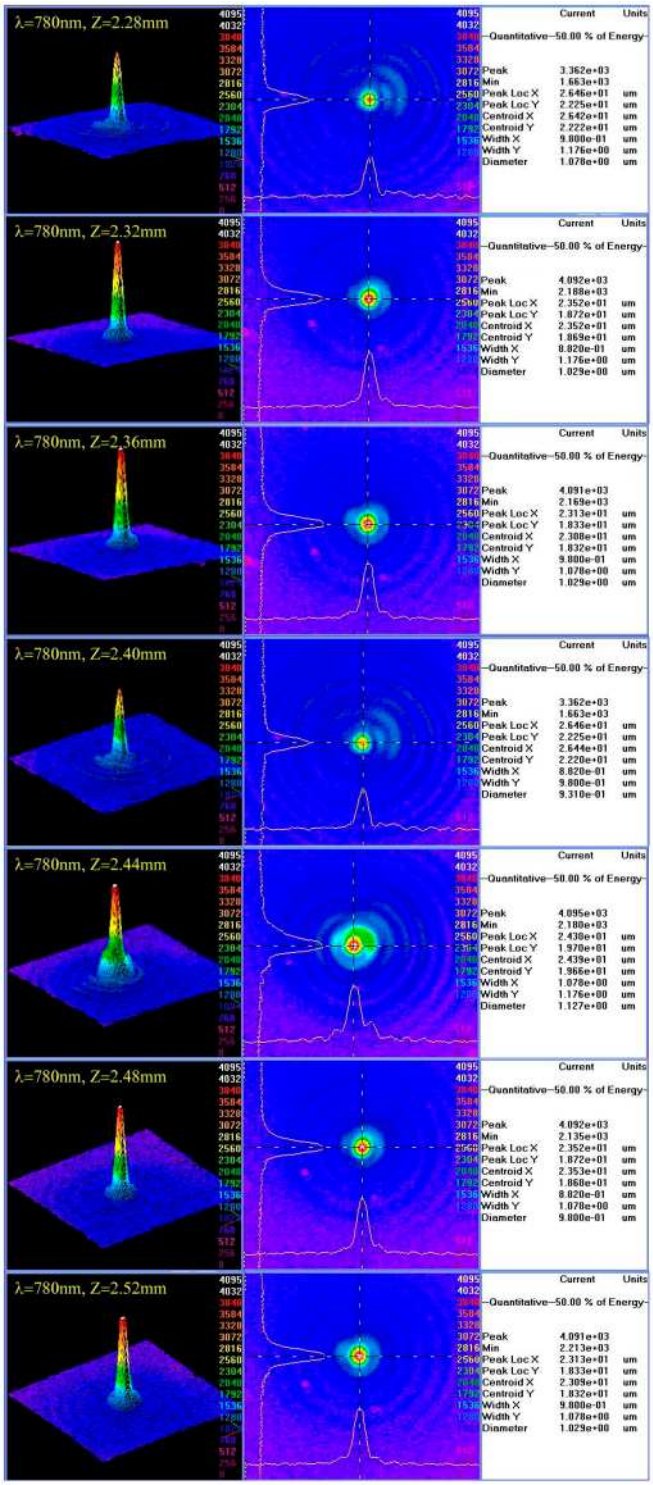

Fig. 16. Photographs present the spot size of the fused-silica-based DOL with dual-wavelength ADDB for FWHM of λ_{CD} segment for a measuring distance of 40 μm per frame.

#119710 - $15.00 USD Received 10 Nov 2009; revised 27 Dec 2009; accepted 7 Jan 2010; published 22 Jan 2010
(C) 2010 OSA

6. Conclusions

In this study we proposed the use of the high-order Bessel modified conjugate-gradient method to a design a fused-silica DOL that can generated a dual-wavelength ADDB for high-NA applications. We have shown that satisfactory banded-krait-like beams with a high transverse resolution approaching the near-zone of the near-field diffraction region could be obtained using a multiple-segment ADDB. The dual-wavelength ADDB was characterized by a segmented axial intensity distribution with a high transverse resolution, and each segment had an extended depth-of-focus and a single wavelength. The results revealed a good transverse intensity distribution and high axial intensity uniformity. Because of some alignment defects, the fabricated fused-silica-based DOL had different spot sizes and lower transverse resolutions than predicted in the simulation. Nevertheless, better results could be obtained by using grey-level laser micromachining or E-beam lithography to produce a smoother profile and achieve higher diffraction efficiency, reducing the spot-size error and improving the transverse resolution. It should be noted that errors in the fabrication resulting from mask misalignments had an obvious influence on the spot signal distribution and axial intensity uniformity. We have seen that the high-order Bessel modified conjugate-gradient method can be a useful and powerful tool in the design of DOLs that generate dual-wavelength and multi-function ADDB that has the potential to match the practical requirements for objective lenses in DVD optical pickup systems. In conclusion, in this paper, a fused-silica DOL with an optimized structure that generated a dual-wavelength ADDB for high-NA applications in DVD optical pickup heads had been successfully designed and fabricated using a modified optimization method and 2-D weighting factor. The results showed an ultra long depth-of-focus, but inadequate lateral resolution, which could be improved by employing better fabrication processes. This implied that the problems associated with the assembly and optical alignment of the many optical elements in a dual-wavelength ADDB DOL can be overcome. Moreover, the increased lateral resolution and expanded longitudinal axial distribution in this fused-silica ADDB DOL had been demonstrated by both theoretical analysis and experimental results.

#119710 - $15.00 USD Received 10 Nov 2009; revised 27 Dec 2009; accepted 7 Jan 2010; published 22 Jan 2010
(C) 2010 OSA